

EPJ D

Atomic, Molecular,
Optical and Plasma Physics

EPJ.org


your physics journal

Eur. Phys. J. D **59**, 209–213 (2010)

DOI: 10.1140/epjd/e2010-00164-x

Experimental and theoretical determination of the stopping power of ZrO_2 films for protons and α -particles

M. Behar, C.D. Denton, R.C. Fadanelli, I. Abril, E.D. Cantero, R. Garcia-Molina and L.C.C. Nagamine



Experimental and theoretical determination of the stopping power of ZrO₂ films for protons and α -particles

M. Behar¹, C.D. Denton^{2,a}, R.C. Fadanelli¹, I. Abril², E.D. Cantero³, R. Garcia-Molina⁴, and L.C.C. Nagamine¹

¹ Instituto de Física, Universidade Federal do Rio Grande do Sul, Av. Bento Gonçalves 9500, 91501-970, Porto Alegre, RS, Brazil

² Departament de Física Aplicada, Universitat d'Alacant, Apartat 90, 03080 Alacant, Spain

³ División de Colisiones Atómicas, Centro Atómico Bariloche, 8400, San Carlos de Bariloche, Argentina

⁴ Departamento de Física - Centro de Investigación en Óptica y Nanofísica (CIOyN), Universidad de Murcia, 30100 Murcia, Spain

Received 30 March 2010 / Received in final form 23 April 2010

Published online 18 June 2010 – © EDP Sciences, Società Italiana di Fisica, Springer-Verlag 2010

Abstract. We report the results of an experimental-theoretical study on the stopping power of ZrO₂ films for swift H and He ion beams. The experiments, using the Rutherford Backscattering technique, were done for protons with incident energies in the range 200–1500 keV and for α -particle beams with energies in the range 160–3000 keV. The theoretical calculations were done in the framework of the dielectric formalism using the MELF-GOS model to account for the ZrO₂ target electronic response. It is shown that for both ion beams, the agreement between theory and experiment is quite remarkable.

1 Introduction

A good control of the energy deposited by an energetic projectile in a given target is extremely important for achieving a reasonable interpretation in ion beam analysis or a satisfactory result in ion beam modification of materials [1]. To this end it is essential to know the quantity of main interest: the stopping power of the target, S , defined as the mean energy lost by the projectile per unit path length inside the target. In the energy range we will consider in this work, the energy lost by a projectile is mainly due to interactions with the target electrons. Therefore a theoretical evaluation of the stopping power must take into account in a realistic way the electronic response of the target to the perturbation caused by the projectile.

The stopping power has been extensively studied both experimentally and theoretically for a number of materials [2]; however, there are limited studies of the stopping power for compound targets. This is due to experimental difficulties in preparing and manipulating compound targets for energy-loss measurements.

Among the compound targets, ZrO₂, also known as zirconia, is one of the most studied ceramic materials due to its wide range of technological applications [3]. ZrO₂ has useful mechanical properties for manufacturing medical devices [4] and very good characteristics for engineering applications [5]. Among other applications ZrO₂ is used in

devices working at high temperatures due to its low thermal conductivity, as a diamond simulant in jewellery or as a refractory material in insulation, abrasives, enamels and ceramic glazes [6,7]. Moreover ZrO₂ is an important high- k dielectric material that is being investigated for potential applications as a gate in future MOSFET transistors [8,9]. Also, ZrO₂ plays an important role in the analysis of the stability against fission fragments of ceramic materials used in inert matrices [10]. Nevertheless, as far as we know, only few papers have been devoted to measure the stopping power of ZrO₂, mainly for heavy ion projectiles [11–14].

In the present communication we report experiments and calculations of the stopping power of ZrO₂ films for proton and for α -particle beams in a large energy interval. The calculations are based on the dielectric formalism and a realistic model to account for the electronic response of the ZrO₂ target to external perturbations.

2 Experimental details and data analysis

The ZrO₂ films were grown on a Si(100) wafer by radio frequency magnetron sputtering using a ZrO₂ target (with a Hf impurity content of 5% wt) and O₂/Ar gas mixture as a sputtering gas. In this way films of thicknesses $t = 18, 35, 58, 82$ and 92 nm were obtained. The thickness of each film was achieved by controlling the deposition time and was further checked by the X-ray reflectivity technique by using the software WinGixa from Philips. In addition

^a e-mail: denton@ua.es

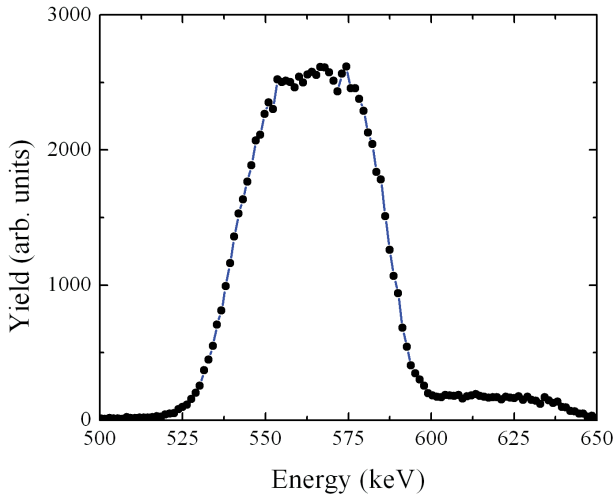


Fig. 1. (Color online) High energy part of the RBS spectrum of a 37 nm thick ZrO_2 film obtained with a 700 keV He ion beam. The step on the right side of the Zr peak corresponds to the Hf component of the target, while the line is only to guide the eye.

this program provides the density of the film, which is 5.6 g/cm^3 (in agreement with the density given by the manufacturer), and the roughness of the films that is typically of 0.5 nm. Further details of the sample preparation and characterization are described in [15]. The typical error in the thickness measurements was of the order of 4% and the stoichiometry of the films was checked and confirmed using the Rutherford backscattering technique (RBS).

For the H ion beam, the interval covered by the present experiment was between 200 and 1500 keV and the detector plus electronic resolution was better than 6 keV (FWHM). On the other hand, for the He ion beam the energy interval covered was between 160 and 3000 keV, the corresponding total resolution being better than 10 keV (FWHM).

The samples were mounted on a four-axis goniometer and the detector was fixed at 120° with respect to the incident beam. For each incident energy, four RBS spectra were recorded at 0° , 20° , 40° , and 60° between the sample surface and the beam direction. The selection of the films was done according to the beam energy. In some cases for a fixed energy we have repeated the experiment with samples of different thickness and the results obtained were quite consistent.

For the data analysis we have used the mean energy approximation, which in the present case is more suitable than the surface one, as described and discussed in reference [16]. Figure 1 shows an RBS spectrum of a 37 nm thick ZrO_2 film obtained with a 700 keV He ion beam. The step on the right side of the Zr peak corresponds to the Hf component of the original target. It should be stressed that the RBS spectrum does not reveal the existence of any other contaminations in the ZrO_2 film. In the mean approximation formalism, for a fixed beam-detector geometry two measurements are necessary at different

beam-sample geometries in order to obtain the stopping power at the inward and outward paths along the sample. In the present case we had four different geometries for the same energy and consequently we have a set of equations from which we can obtain the desired stopping power values with very good precision [15]. Proceeding in this way for each energy, the stopping power data for H and for He projectiles were obtained. The main source of errors is due to the film thickness determination. It should be stated that all the data analysis was performed on the Zr component of the film since the spectrum corresponding to O is superposed on the Si background and hence not well defined.

3 Theoretical description

The theoretical evaluation of the stopping power of ZrO_2 for protons and α -particles has been done using the dielectric formalism [17] and the MELF-GOS model [18,19] to account for the electronic response of the target to external perturbations. The stopping power of a given target for a projectile of charge q and velocity v , S_q , can be obtained within the dielectric formalism as

$$S_q = \frac{2e^2}{\pi v^2} \int_0^\infty d\omega \omega \int_{\omega/v}^\infty \frac{dk}{k} |f_q(k)|^2 \text{Im} \left[\frac{-1}{\varepsilon(k, \omega)} \right]. \quad (1)$$

The target response to an external electromagnetic perturbation is contained in the energy loss function (ELF), $\text{Im}[-1/\varepsilon(k, \omega)]$, which represents the probability for the projectile to produce an electronic excitation of momentum $\hbar k$ and energy $\hbar\omega$ in the material. On the other hand, the projectile nature appears through the Fourier transform of its electronic density, $f_q(k)$, and is modeled here using the Brandt-Kitagawa theory [20].

At high velocities, projectiles are strongly ionized and can be described as point charges without structure. However, at intermediate velocities, electron capture and loss become relevant and different possible charge states of the projectile arise. Therefore the total stopping power, S , will be a weighted sum of the different partial stopping powers corresponding to each charge state q :

$$S = \sum_{q=0}^{Z_1} \phi_q S_q. \quad (2)$$

Here ϕ_q represents the equilibrium q -charge state fractions of the projectile with atomic number Z_1 . We take the ϕ_q values from a parameterization provided by the CasP code [21–23], although it should be noted that for compound targets, such as ZrO_2 films, this code applies Bragg's additivity rule [24] to the target constituents.

The ELF of ZrO_2 is described here using the MELF-GOS model [18,19], which has been successfully applied to calculate the energy loss parameters in compound materials with a complex excitation spectrum [15,25,26], similar to the case of ZrO_2 . This method

Table 1. Parameters used in equation (5) to describe the contribution of the outer electrons to the ELF spectrum of ZrO₂, as explained in the text. The mass density of ZrO₂ is 5.6 g/cm³. The threshold energy is $\hbar\omega_{th,i} = 4$ eV ($i = 1-5$).

i	$\hbar\omega_i$ (eV)	$\hbar\gamma_i$ (eV)	A_i
1	13.06	2.72	8.24×10^{-2}
2	16.87	8.16	1.82×10^{-1}
3	24.49	10.07	2.35×10^{-1}
4	41.36	14.97	2.25×10^{-1}
5	108.85	498.80	9.47×10^{-2}

treats in a different way the contribution to the ELF of the target outer-shell and inner-shell electrons, respectively.

$$\text{Im} \left[\frac{-1}{\varepsilon(k=0, \omega)} \right] = \text{Im} \left[\frac{-1}{\varepsilon(k=0, \omega)} \right]_{outer} + \text{Im} \left[\frac{-1}{\varepsilon(k=0, \omega)} \right]_{inner}. \quad (3)$$

The ELF due to the excitation of outer-shell electrons is obtained via a fitting to the experimental optical-ELF ($k = 0$) through a linear combination of Mermin-type ELFs, namely,

$$\text{Im} \left[\frac{-1}{\varepsilon(k=0, \omega)} \right]_{outer} = \sum_i A_i \text{Im} \left[\frac{-1}{\varepsilon_M(\omega_i, \gamma_i; k=0, \omega)} \right] \quad \text{for } \omega \geq \omega_{th,i}, \quad (4)$$

where ε_M represents the Mermin dielectric function [27], ω_i corresponds to the plasma frequency, γ_i to the width and A_i to the intensity of the most relevant peaks in the experimental energy loss spectrum; $\omega_{th,i}$ is a threshold energy which corresponds to the gap energy of ZrO₂ (~ 4 eV) [28]. The corresponding ELF at $k \neq 0$ is obtained through the properties of the Mermin dielectric function. The optical ELF of ZrO₂ has been taken from reference [29], and it is in general accordance with a more recent determination [30].

The inner-shell electrons are not sensitive to aggregation effects in the compound target and preserve their atomic character. So they are described by their generalized oscillator strengths (GOS) and contribute to the ELF by means of the following expression [31]

$$\text{Im} \left[\frac{-1}{\varepsilon(k, \omega)} \right]_{inner} = \frac{2\pi N}{\omega} \sum_j \alpha_j \sum_{nl} \frac{df_{nl}^{(j)}(k, \omega)}{d\omega}, \quad (5)$$

where N is the molecular density of the target, $df_{nl}^{(j)}(k, \omega)/d\omega$ is the hydrogenic GOS corresponding to the (n, l) -subshell of the j th element, and α_j indicates the stoichiometry of the j th-element in the compound target. For ZrO₂, the electrons from the K-shell of O, as well as the K- and L-shells of Zr are treated as inner electrons.

The method also demands that the resulting ELF will satisfy the f -sum rule [33] for every k value. The parameters of the fitting used in equation (4) appear in Table 1,

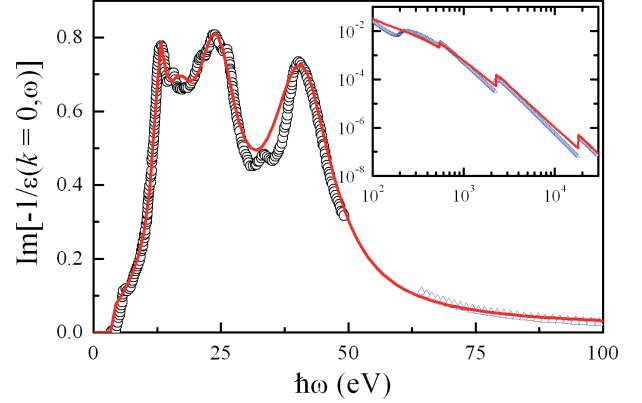


Fig. 2. (Color online) Energy loss function of ZrO₂ as a function of the transferred energy, $\hbar\omega$, in the optical limit ($k = 0$). The circles correspond to experimental data from Frandon et al. [29], the solid line represents the ELF obtained through the MELF-GOS model [18,19] and the triangles (at $\hbar\omega \geq 60$ eV) are data derived from X-ray scattering factors from Henke et al. [32].

and are slightly different from the ones appearing in reference [19] in order to enhance the agreement with the f -sum rule, which is now achieved within 99.9%. Figure 2 shows the ELF of ZrO₂ in the optical limit ($k = 0$). The circles correspond to the experimental data from reference [29], while the line is the ELF resulting from the MELF-GOS model. The ELF at high values of ω compares satisfactorily with the data obtained from X-ray scattering factors represented by triangles [32].

4 Results and conclusions

The stopping power S of ZrO₂ films is represented in Figures 3 and 4 for H and He ion beams as a function of the incident energy. The full circles correspond to the measured experimental results whereas the full lines represent the theoretical calculation with the MELF-GOS model. In the right axis of both figures we also show the stopping cross section SCS , defined as $SCS = S/N$, with N being the molecular density. As can be observed for both projectiles the theoretical-experimental agreement is quite good, despite the large energy interval covered in the present study. In the case of He ions the energy range of the experiments includes the maximum of the stopping power.

We have also included in the figures the predictions of the SRIM-2008 code [34,35]. These results differ from the MELF-GOS calculations, in particular in the energy range corresponding to the stopping power maximum. These differences represent $\sim 20\%$ of the stopping power for H ion projectiles and $\sim 15\%$ for He ion projectiles. Note that when no experimental results are available SRIM obtains the stopping power of compounds by applying Bragg's additivity rule. In the case of certain compounds of light atoms, SRIM does offer corrections from Bragg's additivity rule, but for compounds with heavier

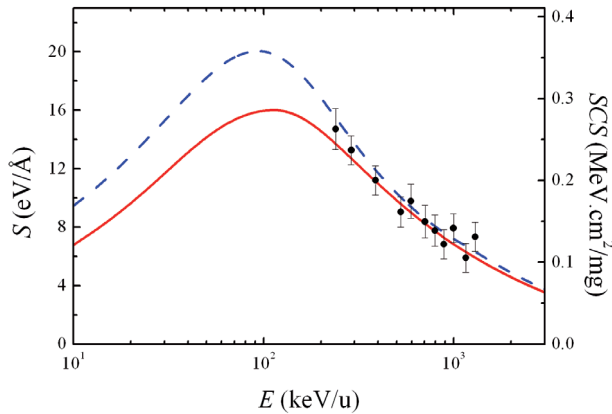


Fig. 3. (Color online) Stopping power (left axis) of a ZrO_2 film for a proton beam as a function of the incident energy. The symbols represent the experimental results, the full line represents our theoretical calculation using the MELF-GOS model and the dashed line is the prediction of the SRIM-2008 code [34,35]. The right axis represents the stopping cross section.

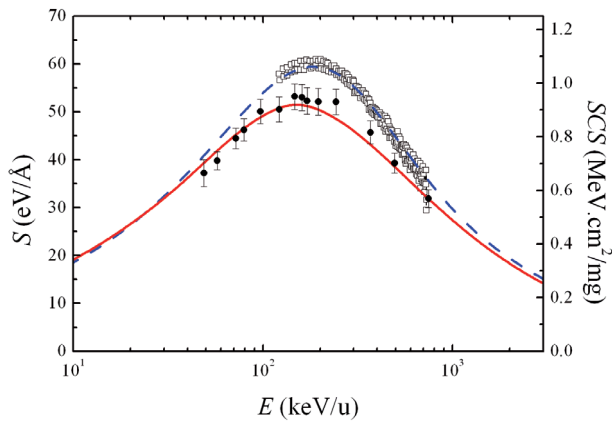


Fig. 4. (Color online) Stopping power (left axis) of a ZrO_2 film for an α -particle beam as a function of the incident energy. The full circles stand for the experimental results obtained in this work, open squares correspond to previous experiments with an error of 4% [13], the full line represents our theoretical calculation using the MELF-GOS model and the dashed line is the prediction of the SRIM-2008 code [34,35]. The right axis represents the stopping cross section.

constituents like Zr, SRIM assumes that no correction is necessary ignoring thus aggregation effects [36]. As far as we know, there are no experimental data of stopping power of ZrO_2 for protons available, while there are two previous measurements for He ion projectiles [12,13]. We will not discuss the first set of data [12] because the authors used He^3 instead of He^4 and the energy scale was not adequate [37]. On the other hand the results of reference [13] are represented by empty squares in Figure 3, and show a good agreement with SRIM predictions. Currently we do not have a plausible explanation for the experimental discrepancies between measurements reported in the present work and the results of reference [13]. However it should be stressed that in reference [13] the film thickness was

obtained by normalizing to the SRIM results the energy loss of α -particles through the ZrO_2 films over a wide energy region [12], while in the present case we have used an independent measuring technique to determine the thickness of the film.

The mean excitation energy, I , calculated for ZrO_2 with the dielectric formalism together with the MELF-GOS model has a value of 377 eV, which is noticeably larger than the value of 295 eV derived by interpolation from the ICRU report 49 [38]. This I value is essential to determine the behaviour of the stopping power at high energies using the Bethe formula [39]. This difference in the I values represents a variation of 8% in the stopping power of ZrO_2 for a proton beam at 3000 keV/u.

In summary, we report new measurements of the stopping power of ZrO_2 films for H and He ion beams, by using the RBS technique. The projectile energies studied here range from 200 to 1500 keV for proton beams and from 160 to 3000 keV for alpha beams. The theoretical calculations using the dielectric formalism together with the MELF-GOS model show good agreement in the whole range of projectile energies, in particular for He ions where the maximum is well reproduced. This feature is a real challenge for any theoretical-experimental work. This agreement is founded in a realistic description of the target electronic response as provided by the MELF-GOS model.

This work has been financially supported by the Brazilian CNPq Agency (Contract 150757/2007). EDC acknowledges support from the Consejo Nacional de Investigaciones Científicas y Técnicas (CONICET), Argentina.

References

1. M. Nastasi, J.W. Mayer, J.K. Hirvonen, *Ion-Solid Interactions: Fundamentals and Applications* (Cambridge University Press, Cambridge, 1996)
2. H. Paul, Stopping power of light ions. Available at <http://www.exphys.uni-linz.ac.at/stopping/>
3. V. Milman, A. Perlov, K. Refson, S.J. Clark, J. Gavartin, B. Winkler, *J. Phys. Cond. Mat.* **21**, 485404 (2009)
4. P.F. Manicone, P.R. Iommetti, L. Raffaelli, *J. Dent.* **35**, 819 (2007)
5. M.H. Bocanegra-Bernal, S.D. de la Torre, *J. Mater. Sci.* **37**, 4947 (2002)
6. A.H. Heuer, L.W. Hobbs, *Science and Technology of Zirconia, Advances in Ceramics*, edited by A.H. Heuer, L.W. Hobbs (The American Ceramic Society, Columbus, OH, 1981), Vol. 3
7. N. Claussen, M. Rühle, A.H. Heuer, *Science and Technology of Zirconia II, Advances in Ceramics*, edited by N. Claussen, M. Rühle, A.H. Heuer (The American Ceramic Society, Columbus, OH, 1984), Vol. 12
8. M. Houssa, *High-k gate dielectrics. Series in Material Science and Engineering*, edited by M. Houssa (Institute of Physics Publishing, Bristol, 2004)

9. H. Jin, S.K. Oh, H.J. Kanga, S. Tougaard, *J. Appl. Phys.* **100**, 083713 (2006)
10. G. Szenes, *J. Nucl. Mat.* **336**, 81 (2005)
11. K. Arstila, *NIM B* **168**, 473 (2000)
12. Y. Zhang, J. Jensen, G. Possnert, D.A. Grove, D.E. McCready, B.W. Arey, W.J. Weber, *NIM B* **249**, 18 (2006)
13. Y. Zhang, W.J. Weber, *NIM B* **267**, 1705 (2009)
14. M. Msimanga, C.M. Comrie, C.A. Pineda-Vargas, S. Murray, R. Bark, G. Dollinger, *NIM B* **267**, 2671 (2009)
15. M. Behar, R.C. Fadanelli, I. Abril, R. Garcia-Molina, C.D. Denton, L.C.C.M. Nagamine, N.R. Arista, *Phys. Rev. A* **80**, 062901 (2009)
16. W.K. Chu, J.W. Mayer, M.A. Nicolet, *Backscattering Spectrometry* (Academic Press, New York, 1978)
17. J. Lindhard, K. Dan, *Vidensk. Selsk. Mat. Fys. Medd.* **28**, No. 8 (1954)
18. I. Abril, R. Garcia-Molina, C.D. Denton, F.J. Pérez-Pérez, N.R. Arista, *Phys. Rev. A* **58**, 357 (1998)
19. S. Heredia-Avalos, R. Garcia-Molina, J.M. Fernández-Varea, I. Abril, *Phys. Rev. A* **72**, 052902 (2005)
20. W. Brandt, M. Kitagawa, *Phys. Rev. B* **25**, 5631 (1982)
21. G. Schiwietz, P.L. Grande, *NIM B* **175**, 125 (2001)
22. G. Schiwietz, K. Czernski, M. Roth, F. Staufenbiel, P.L. Grande, *NIM B* **226**, 683 (2004)
23. P.L. Grande, G. Schiwietz, CasP code, Convolution Approximation for Swift Particles, version 3.1, 2005. Available at http://www.helmholtz-berlin.de/people/gregor-schiwietz/casp_en.html
24. W.H. Bragg, R. Kleeman, *Phil. Mag.* **10**, 318 (1905)
25. I. Abril, R. Garcia-Molina, N.R. Arista, C.F. Sanz-Navarro, *NIM B* **190**, 89 (2002)
26. R. Garcia-Molina, I. Abril, C.D. Denton, S. Heredia-Avalos, I. Kyriakou, D. Emfietzoglou, *NIM B* **267**, 2647 (2009)
27. N.D. Mermin, *Phys. Rev. B* **1**, 2362 (1970)
28. D.W. McComb, *Phys. Rev. B* **54**, 7094 (1996)
29. J. Frandon, B. Rousseau, F. Pradal, *Phys. Stat. Sol. B* **98**, 379 (1980)
30. F. Yubero, J.M. Sanz, J.F. Trigo, E. Elizalde, S. Tougaard, *Surf. Interface Anal.* **22**, 124 (1994)
31. U. Fano, *Annu. Rev. Nucl. Sci.* **13**, 1 (1963)
32. B.L. Henke, E.M. Gullikson, J.C. Davis, *At. Data Nucl. Data Tables* **54**, 181 (1993)
33. E. Shiles, T. Sasaki, M. Inokuti, D.Y. Smith, *Phys. Rev. B* **22**, 1612 (1980)
34. J.F. Ziegler, J.P. Biersack, M.D. Ziegler, *SRIM. The Stopping and Range of Ions in Matter* (Maryland, 2008)
35. J.F. Ziegler, J.P. Biersack, SRIM-2008, The Stopping and Range of Ions in Matter, Version 2008. Available at <http://www.srim.org>
36. H. Paul, A. Schinner, *NIM B* **249**, 1 (2006)
37. Y. Zhang, private communication
38. ICRU Report 49, *Stopping Powers and Ranges for Protons and Alpha Particles*, International Commission on Radiation Units and Measurements, Bethesda, Maryland, 1994, Vol. 49
39. H. Bethe, *Ann. Phys. Lpz.* **5**, 325 (1930)